Impurity structure in a molecular ionic crystal: Atomic-scale x-ray study of $CaCO_3:Mn^{2+}$

L. Cheng

Environmental Research Division, Argonne National Laboratory, Argonne, Illinois 60439
and Department of Materials Science and Engineering, Northwestern University, Evanston, Illinois 60208

N. C. Sturchio

Department of Earth and Environmental Sciences, University of Illinois at Chicago, Chicago, Illinois, 60607
and Environmental Research Division, Argonne National Laboratory, Argonne, Illinois 60439

M. J. Bedzyk

Department of Materials Science and Engineering and Institute of Environmental Catalysis, Northwestern University,
Evanston, Illinois 60208

The lattice sites and spatial disorder of isolated Mn^{2+} ions in calcite were examined with x-ray standing waves, and the structure of the surrounding ions was examined with extended x-ray absorption fine-structure spectroscopy. The Mn^{2+} ion is found to be on-center substitutional at the Ca^{2+} site, with spatial disorder comparable to that of Ca^{2+}. The first-neighbor Mn-O distance is found to be the same as that in the isostructural $MnCO_3$. The radial distance of the closest Mn-Ca shell is reduced by $\sim 2\%$ from the undistorted Ca-Ca distance. Based on these measurements, an atomic-scale structural model of the Mn^{2+} site suggests that the intramolecular distortion in the first-neighbor CO_3^{2-} anions plays a key role in establishing the conserved first-neighbor Mn-O distance while maintaining ordering with respect to the lattice. The $CaCO_3:Mn^{2+}$ structure is shown to be characteristically distinct from those of analogous impurities in monatomic ionic crystals.

PACS number(s): 61.72.Dd

I. INTRODUCTION

The structure of an impurity atom site in a crystal reflects impurity-lattice interactions. Correlations are often found between impurity structures and crystal properties or impurity processes.[1] Extensive experimental and computational work has been done on impurity-induced structural distortions in monatomic crystals, including the ionic crystals of alkali halides[2–5] and ABO_3-type oxides,[6] and the covalent semiconductor crystals of the diamond[7,8] and zinc-blende[7,9] structures. Much less understood, however, are impurity structures in molecular ionic crystals. In these crystals, impurities are expected to have more complex structures due to the interplay between interionic and intramolecular relaxations. Recently, extended x-ray absorption fine structure spectroscopy (EXAFS) studies on isolated Zn^{2+}, Co^{2+}, and Ni^{2+} in the bulk[10] and surface[11–13] lattices of calcite ($CaCO_3$) were reported. These divalent cations form carbonates having a calcite structure; their substitutions of Ca^{2+} in calcite (hereafter denoted as $CaCO_3:M$) retain much of the local symmetry of the host, favorable for unambiguous structural determination. A notable feature of these impurity systems is that the bond distance between M and its nearest-neighbor O atoms is the same as in the respective MCO_3 pure crystals. Such a feature, often referred to as first-neighbor bond distance conservation, is not characteristic of impurities in monatomic crystals.

We report here an x-ray standing wave (XSW) and an EXAFS study on isolated Mn^{2+} in calcite. Like Ca^{2+}, Mn^{2+} forms a carbonate having the calcite structure. Substitutional Mn^{2+} has been used to probe electronic properties such as spin-lattice interactions in calcite[14] and electron wave func-

tions in semiconductor quantum wells.[15] Here, Mn^{2+} acts as a structural probe of local lattice distortion. The site(s), spatial disorder and potential positional displacement of the Mn^{2+} ion are determined with XSW, while the relaxations of the surrounding CO_3^{2-} and Ca^{2+} ions are determined with EXAFS. Through these atomic-scale measurements, we aim to identify the structural characteristics that distinguish the $CaCO_3:M$ system from analogous impurity systems in monatomic ionic crystals. In particular, this helps understand trace-aqueous-ion incorporation at the water-calcite interface, a process fundamental to the geochemical and environmental problems of trace-element partitioning.[16]

II. EXPERIMENT

The x-ray measurements were made at the National Synchrotron Light Source (NSLS), at beamline X15A, with a double-crystal monochromator and a four-circle diffractometer. The $CaCO_3:Mn^{2+}$ sample was a single crystal calcite containing 0.0006 Mn^{2+} per Ca^{2+}, as determined by inductively coupled plasma atomic-emission spectrometry. The calcite structure has rhombohedral (hexagonal) symmetry, space group $R\bar{3}c$, with two nonequivalent Ca^{2+} sites per primitive unit cell. Each Ca^{2+} site is octahedrally coordinated to six O atoms of the neighboring CO_3^{2-} anions [Fig. 1(a)]. The sample crystal was cleaved along the $(10\bar{1}4)$ face for the XSW measurements, and was in a fine-powder form for the EXAFS measurements. Both the XSW and EXAFS measurements were made at room temperature. The XSW measurements were made with x rays of 9.00 keV on the calcite $(10\bar{1}4)$ and $(20\bar{2}8)$ Bragg reflections using a pair of
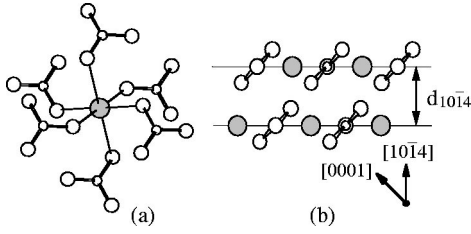
FIG. 1. The Ca^{2+} site in calcite: (a) the octahedral near-neighbor coordination of the Ca^{2+} site and (b) the location of Ca^{2+} relative to the $(10\bar{1}4)$ lattice planes. Shaded circles are Ca, small and large hollow circles are C and O, respectively.

Si(111) and a pair of Si(004) monochromator crystals, respectively, at 75% intensity detune. To minimize dispersion, the monochromator crystals were matched in lattice spacing to that of the sample reflections (to within 3% and 10%, respectively), and the first monochromator crystal was miscut. (The remaining, very slight dispersion was to be taken into account in data analysis.) While stepping up in angle through the Bragg reflections, the fluorescence spectra containing the Mn and Ca emissions were recorded with a solid-state detector. The emission angle was controlled with a slit to eliminate the extinction effect.[17] The EXAFS data were collected in fluorescence mode at the Mn K edge by monitoring the Mn $K\alpha$ emission line over the energy range 6490–7090 eV, using a Ge(111) monochromator at 75% detune. Data for a powdered $MnCO_3$ experimental standard were acquired in transmission mode over the same energy range.

III. RESULTS

A. XSW results

The XSW results are shown in Fig. 2 and listed in Table I. The structural parameters obtained from an XSW are the coherent position P_H and the coherent fraction f_H for the
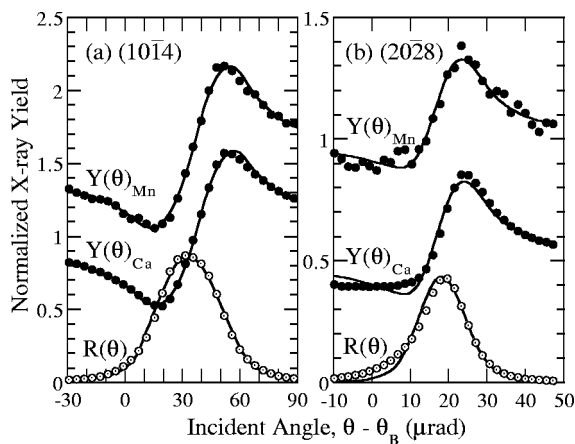

FIG. 2. XSW results. Data (dots) and theoretical fits (solid curves) of the normalized x-ray reflectivity R, and Ca $K(\alpha$ and $\beta)$ and Mn $K\alpha$ fluorescence yields Y for (a) the $(10\bar{1}4)$ and (b) the $(20\bar{2}8)$ Bragg reflections of calcite. The statistical error bars in the data are comparable in size to the data symbols. For clarity of display, Y_{Mn} is vertically offset by 0.5 in (a) and Y_{Ca} by -0.5 in (b).

TABLE I. The best-fit XSW coherent positions P_H and fractions f_H for Ca^{2+} and Mn^{2+}.

Ion	$P_{10\bar{1}4}$	$P_{20\bar{2}8}$	$f_{10\bar{1}4}$	$f_{20\bar{2}8}$
Ca^{2+}	0.00[a]	0.00[a]	0.79±0.01	0.59±0.01
Mn^{2+}	0.01±0.01	0.01±0.01	0.79±0.02	0.54±0.02

[a]These values were held fixed during fits.

$H=hkil$ Bragg reflection. The coherent position is the average position of the probed atoms in units of lattice spacing d_H. The coherent fraction is a measure of the distribution of the atoms about their average position. These two parameters are obtained from the best fits of the theoretical yields (Eq. 1 in Ref. 18) to the normalized experimental Mn $K\alpha$ and Ca $K(\alpha$ and $\beta)$ x-ray fluorescence yields. The fluorescence emission angle with respect to the sample surface, an additional parameter in the yield equation, was determined by an analytical method[18] using the known P_H for Ca^{2+} from the calcite crystal structure.[19]

B. EXAFS results

The $CaCO_3:Mn^{2+}$ EXAFS data were fitted according to standard procedures,[20] in both a Mn-O first-shell fit with respect to the $MnCO_3$ experimental standard (using the MACXAFS 3.6 fitting program[21]) and in a four-shell fit with theoretical amplitudes and phases generated with the FEFF 7.0 program[22] (using the FEFFIT 2.32 fitting program[23]). For the first-shell fit, the background-removed, k^2-weighted $\chi(k)$ data for the $MnCO_3$ standard [Fig. 3(a)] and for the $CaCO_3:Mn^{2+}$ sample [Fig. 3(b)] were Fourier-transformed into R-space over the range $k=2.29-11.71$ Å^{-1} with lower- and upper-modified Hanning windows of $\Delta k=0.5$ and 1.9 Å^{-1}, respectively. The Mn-O first-shell components were filtered over the range $R=1.11-2.14$ Å with $\Delta R=0.14$ Å windows. The back-transformed first-shell $CaCO_3:Mn^{2+}$ data were fitted with respect to the $MnCO_3$ data in radial distance R, coordination number N, and rms vibrational amplitude σ. The final fit was done with $N=6$ held fixed, and at an optimal edge-energy shift value ΔE_0. The filtered first-shell $CaCO_3:Mn^{2+}$ data and its best-fit curve are shown in Fig. 3(b); the best-fit parameters are listed in Table II.

For the multiple-shell fit, isostructural considerations were made to restrict the number of floating parameters in order to avoid parameter-correlation-caused unrealistic results. The theoretical $MnCO_3$ $\chi(k)$ function composed of the four most significant single-scattering paths [O(1), C(1), O(2), Mn(1)] was fitted in k^3 weight (in order to enhance outer-shell signals) to the experimental $MnCO_3$ data in back-transformed k-space.[24] The forward- and back-Fourier-transform ranges and windows were: $k=2.3-11.00$ Å^{-1}, $\Delta k=0.5$, and 1.9 Å^{-1}; $R=0.8-4.0$ Å, $\Delta R=0.14$ Å. The data and the best fit are shown in Fig. 3(c); the latter reproduced the $MnCO_3$ structure within expected uncertainties (Table II), hence validating the four-shell model. The fit gave $\Delta E_0=0.65\pm3.20$ eV and the amplitude-reduction factor $S_0^2=0.71\pm0.21$. With the optimal values of ΔE and S_0^2, a the-
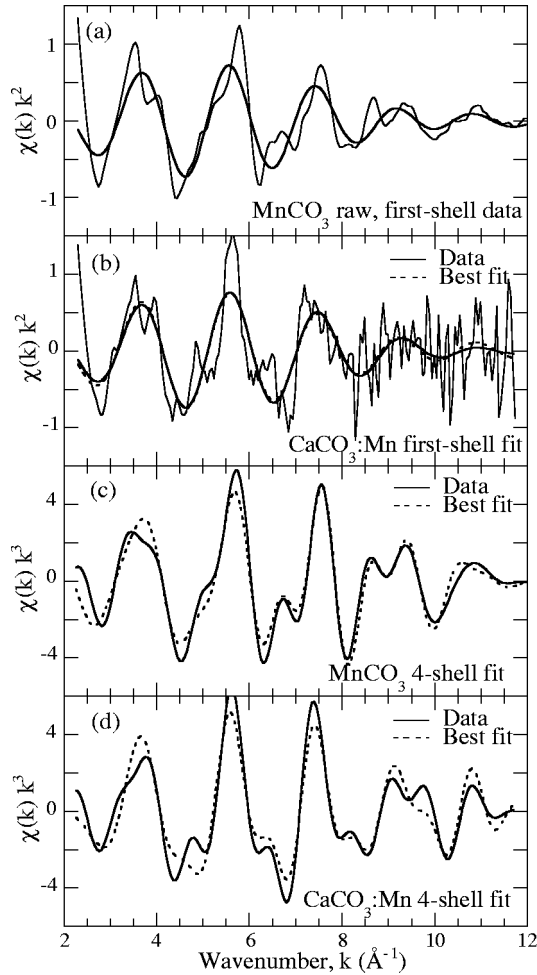
FIG. 3. EXAFS results. (a) The k^2-weighted raw and first-shell data for the $MnCO_3$ experimental standard, (b) the k^2-weighted raw and first-shell data and fit for $CaCO_3:Mn^{2+}$, (c) the k^3-weighted four-shell data and fit for $MnCO_3$, and (d) the k^3-weighted four-shell data and fit for $CaCO_3:Mn^{2+}$.

TABLE II. The best-fit EXAFS values of radial distances R and rms vibrational amplitudes σ from the $MnCO_3$ four-shell fit, the $CaCO_3:Mn^{2+}$ first-shell fit, and the $CaCO_3:Mn^{2+}$ four-shell fit (N fixed at 6). Also listed for comparison are the R values for corresponding atom shells in pure $MnCO_3$ and $CaCO_3$.

Shell	Pure crystal	EXAFS-measured	
	R (Å)	R (Å)	σ (Å)
	$MnCO_3$	$MnCO_3$ four-shell fit	
O(1)	2.19	2.19 ± 0.02	0.08 ± 0.05
C(1)	3.05	3.09 ± 0.09	0.11 ± 0.10
O(2)	3.31	3.34 ± 0.07	0.11 ± 0.10^a
Mn(1)	3.79	3.80 ± 0.03	0.10 ± 0.06
	$CaCO_3$	$CaCO_3:Mn^{2+}$ first-shell fit	
O(1)	2.36	2.18 ± 0.01	0.09 ± 0.05
	$CaCO_3$	$CaCO_3:Mn^{2+}$ four-shell fit	
O(1)	2.36	2.18 ± 0.02	0.08 ± 0.04
C(1)	3.21	3.46 ± 0.10	0.05 ± 0.07
O(2)	3.46	3.63 ± 0.08	0.05 ± 0.07^a
Ca(1)	4.05	3.96 ± 0.04	0.08 ± 0.05

^{a}The σ values for O(2) and C(1) were held equal during fits.

oretical $CaCO_3:Mn^{2+}$ four-shell model analogous to the $MnCO_3$ model was fitted in k^3 weight to the experimental $CaCO_3:Mn^{2+}$ data in back-transformed k-space with the same forward- and back-transform ranges and windows. The data and the best fit are shown in Fig. 3(d), the best-fit parameters are listed in Table II.

IV. DISCUSSION

A. XSW: On-center substitution of Mn

The use of XSW to determine impurity sites in crystals has been demonstrated in several reports.[25–28] Referring to Fig. 1(b), the mean position of an atom relative to the calcite $(10\bar{1}4)$ plane is $h_{10\bar{1}4} = d_{10\bar{1}4}P_{10\bar{1}4}$. With one of the carbon sites chosen as the origin, the Ca^{2+} ions are located at $h_{10\bar{1}4} = 0$. From the XSW analysis [Fig. 2(a) and Table I], the Mn^{2+} ions have a height of $h_{10\bar{1}4} = 0.03 \pm 0.03$ Å. By symmetry of the calcite structure, the $(10\bar{1}4)$ planes are equivalent to the noncoplanar $(\bar{1}104)$ and $(0\bar{1}14)$ planes. This implies that $h_{\bar{1}104} = h_{0\bar{1}14} \sim 0$ for Mn^{2+} as well. Therefore,

Mn^{2+} is located at the Ca^{2+} crystallographic sites, in agreement with a previous XSW result.[29]

For substitutional cations smaller than the host ion, displacements to off-center positions are common in alkali halides[2,3] and the ABO_3 oxides (e.g., Li^+ in $KTaO_3$).[6] Whether off-center displacement also occurs for cation impurities in calcite is not completely clear. The $CaCO_3:Mn^{2+}$ system is one in which the impurity is smaller than the host, with ratio of their ionic radii $r_{Mn^{2+}}/r_{Ca^{2+}} = 0.81$. In the XSW analysis, off-center positions can be specified with the geometric factor in the coherent fraction, and the displacement distances can then be quantitatively solved. This analysis, however, requires knowing the other factors in the coherent fraction, namely, the ordered fraction and the Debye-Waller factor; these factors can be resolved with multiple-order measurements in $\langle H \rangle$. This analysis also relies on a realistic model of the displacement geometry.

For Mn^{2+} in calcite, we find that its $f_{10\bar{1}4}$ and $f_{20\bar{2}8}$ values are approximately equal to those for Ca^{2+} (Table I); this indicates that the Mn^{2+} substitution is on center. In contrast, assuming an off-center displacement of a typical amplitude of ~ 0.5 Å for polarizable cations,[2,3,6] a significantly reduced, coherent fraction would be found for the impurity than for the host ion.

B. EXAFS: Conserved first-neighbor Mn-O distance

The EXAFS analysis determines that the first-neighbor Mn-O(1) bond distance in $CaCO_3:Mn^{2+}$ is the same as that in $MnCO_3$ (Table II). This first-neighbor distance conservation agrees with EXAFS results on several other cation impurities whose carbonates are isostructural to calcite. These are the calcite bulk impurities of Zn^{2+} at concentration $x = 0.00025$ and Co^{2+} at $x = 0.0058$,[10] and the calcite surface

TABLE III. The relaxation parameter ϵ for the O(1) shell and the fractional change in radial distance $\Delta R/R$ for the Ca(1) shell for various cation impurities in calcite, calculated from EXAFS data.

M	r_M/r_{Ca}	ϵ	$\Delta R/R$
Mn^{2+} in bulk [a]	0.81	1.06 ± 0.06	-0.022
Zn^{2+} in bulk [b]	0.75	0.96 ± 0.08	-0.027
Zn^{2+} on surface [c]		1.04 ± 0.04	
Co^{2+} in bulk [b]	0.73	0.96 ± 0.08	-0.030
Co^{2+} on surface [d]		0.96 ± 0.08	
Ni^{2+} on surface [e]	0.70	1.00 ± 0.08	

[a]This study.
[b]Reference 10; for ϵ calculations, single-shell-fit data were used.
[c]Reference 11.
[d]Reference 12.
[e]Reference 13.

impurities of Zn^{2+} at surface coverage $x=0.09$,[11] Co^{2+} at $x=0.05$,[12] and Ni^{2+} at a low submonolayer coverage.[13]

The extent of first-neighbor relaxation surrounding an impurity is often described with a relaxation parameter ϵ defined as the ratio of the relaxed distance to the difference between end-member crystal distances. For a cation impurity system $A^+X^-:M^+$, for example,

$$\epsilon = \frac{R_{M\text{-}X} - R^0_{A\text{-}X}}{R^0_{M\text{-}X} - R^0_{A\text{-}X}}, \tag{1}$$

where the zero-superscripted distances refer to the pure-crystal values. In Eq. (1), the value of ϵ lies between 0 [the virtual crystal approximation (VCA) limit] when unrelaxed, and 1 (the Pauling limit) when fully relaxed. For the typical alkali-halide system of $KBr:Rb^+$, for example, $\epsilon = 0.5-0.54$.[4,5] For the zinc-blende covalent semiconductors, $\epsilon = 0.6-0.8$.[7,9] In general, in both monatomic ionic and covalent systems, the impurity first-neighbor ϵ values fall between the VCA and the Pauling limits.

For $CaCO_3:M$, ϵ can be specifically written as

$$\epsilon = \frac{R_{M\text{-}O(1)} - R^0_{Ca\text{-}O(1)}}{R^0_{M\text{-}O(1)} - R^0_{Ca\text{-}O(1)}}. \tag{2}$$

The ϵ values for Mn^{2+} and the other similar impurities in calcite are calculated from their M-O(1) distances and listed in Table III. The M-O(1) first-neighbor distance conservation is indicated by $\epsilon = 1$. This structural feature contrasts those in monatomic ionic crystals discussed above, for which $\epsilon < 1$.

To determine the criteria for impurity first-neighbor distance conservation, we observe two notable structural characteristics that distinguish the calcite impurities discussed here from other ionic impurity systems in which first-neighbor distance conservation is not found. The first is the match between the preferred chemical structure of the impurity and the coordination environment of the site. This requires that the sizes of the impurity and the host ions be comparable and their valences identical. To illustrate this point, consider the first-neighbor structures of the Pb^{2+},
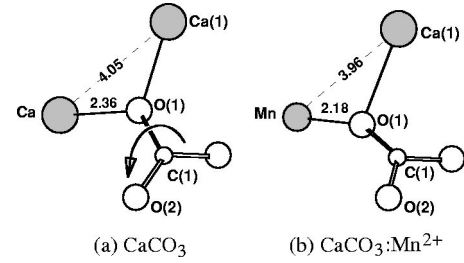

FIG. 4. Structures of the CO_3^{2-} anion (a) surrounding a Ca^{2+} in ideal calcite and (b) surrounding a Mn^{2+} impurity in calcite according to EXAFS radial-distance data. For clarity, only one of the six CO_3^{2-} anions is shown.

Ba^{2+}, and Sr^{2+} in calcite.[10,30] Although these impurities are isovalent to Ca^{2+}, their larger sizes prefer a coordination of nine O atoms compared to that of six O for Ca^{2+}. Therefore, $\epsilon < 1$ is found for these cations in calcite. On the other hand, for substitutional U^{4+} in calcite, the ionic sizes are well matched ($r_{U^{4+}}/r_{Ca^{2+}} = 0.9$), but the mismatch in valence results in a more complex, nonconserved first-neighbor U-O(1) shell.[31]

C. EXAFS: Intramolecular relaxation of CO_3 anions

For cation impurities in monatomic crystals, however, even isostructural substitution may not result in first-neighbor distance conservation. This leads us to the second distinguishing feature of the calcite impurities, which is the large local relaxation. To locate the source of this relaxation, we note that the Mn-Ca(1) distance is not markedly different from that of Ca-Ca(1) in undistorted calcite (Table II). In general, the fractional change $\Delta R/R$ for the Ca(1) shell, defined as

$$\frac{\Delta R}{R} = \frac{R_{M\text{-}Ca(1)} - R_{Ca\text{-}Ca(1)}}{R_{Ca\text{-}Ca(1)}} \tag{3}$$

is only 2–3 % (Table III). This indicates that the position of the Ca(1) shell is determined mainly by the lattice structure of calcite. For $CaCO_3:Mn^{2+}$ in particular, the structure of the Mn^{2+} site undergoes a transition from being dominated by the Mn^{2+} chemical preference at the O(1) shell, to being dominated by the lattice structure at the Ca(1) shell. Obviously, this transition occurs within the first-neighbor CO_3^{2-} anions.

A structural model for the distorted CO_3^{2-} anion can be constructed from the EXAFS radial distance data of the O(1), C(1), and O(2) shells. This model, shown in Fig. 4, allows displacements and bond bending for CO_3^{2-}. It is constructed by first slightly rotating the O(1)-C(1) bond about C(1) (indicated with an arrow in the figure) so that the Mn-O(1) distance reaches its measured value of 2.18 Å, followed by changing the Mn-O(1)-C(1) and the O(1)-C(1)-O(2) bond angles so that the Mn-C(1) and the Mn-O(2) distances also match their measured values of 3.46 Å and 3.63 Å, respectively. As a result of this distortion, the Mn-O(1)-C(1) bond angle is changed from 121° to 141°. The O(1)-

C(1)-O(2) bond angle is also likely to have changed, but its exact value depends on the extent of out-of-plane bending of the now presumably nonplanar CO_3^{2-}. Furthermore, assuming the conserved O(1)-Ca(1) distance of 2.36 Å, the Mn-O(1)-Ca(1) angle is 121°, very close to the Ca-O(1)-Ca(1) angle of 118.6° in ideal calcite; this is consistent with the notion that distortion beyond the first-neighbor CO_3^{2-} is small.

This model shows that the first-neighbor CO_3^{2-} are rotated and distorted to provide the necessary relaxation for O(1) to be bonded to the smaller Mn^{2+}, while preserving bonding to outer-shell Ca^{2+} ions. This satisfies both the chemical bonding on the impurity and the lattice structure of the host crystal. The XSW finding of highly ordered, on-center Mn^{2+} is consistent with this structural interpretation based on the EXAFS data. In contrast, in monatomic ionic crystals, without the option of intramolecular relaxation, energy minimization at the impurity site relies solely on interionic relaxations. These relaxations alone may not be sufficient to accommodate all the strains without noticeably compromising ion positions, resulting in impurity off-center displacements[2] and, at higher impurity concentrations, extended buckling of the crystal lattice.[32]

The calcite impurity systems are expected to have thermodynamic properties quite different from those of monatomic crystals. For example, with on-center substitution, the impurity is expected to be free of off-center effects such as tunneling among off-center sites[33] and off-center-related diffusion,[34] which are present for impurities in monatomic ionic crystals. Furthermore, the confinement of impurity strains by CO_3^{2-} may reduce interactions among impurities, rendering the crystal less susceptible to impurity concentration-dependent processes. In particular, the calcite surface is thought to possess a certain degree of selectivity when adsorbing impurity ions from an aqueous phase, based on ionic size and valence.[35] The criteria for impurity first-neighbor distance conservation discussed here are likely to be fundamentally linked to the structural basis of the adsorption selectivity property of the calcite surface.

V. SUMMARY

Using the XSW and EXAFS, we determined the structure of an Mn^{2+} impurity in calcite. We showed that Mn^{2+} is on-center, with spatial disorder not significantly different from the host Ca^{2+}. The Mn-O(1) first-neighbor distance conservation—a distinct feature found in all $CaCO_3:M$ systems—is attributed largely to the relaxation of the neighboring CO_3^{2-} anions.

Recently developed empirical calcite interatomic-potential functions[36,37] have led to atomistic simulation of impurity structures in calcite.[37] The high-resolution experimental structural data presented here are useful for refining these potentials. Improved potentials enhance simulation accuracy, which, in turn, helps determine certain experimentally unresolved features (e.g., in $CaCO_3:Mn^{2+}$ the position of the most distant O shell in CO_3^{2-}). The combination of atomistic simulation with the XSW and EXAFS would offer a suite of complementary high-resolution methods for impurity structural determination.

[1] *Point Defects in Materials*, edited by F. Agullo-Lopez, C. R. A. Catlow, and P. D. Townsend (Academic Press, London, 1988).

[2] A. S. Barker and A. J. Sievers, Rev. Mod. Phys. **47**, Suppl. 2, FS1 (1975).

[3] C. R. A. Catlow, K. M. Diller, M. J. Norgett, J. Corish, B. Parker, and P. Jacobs, Phys. Rev. B **18**, 2739 (1978).

[4] J. B. Boyce and J. C. Mikkelson, Phys. Rev. B **31**, 6903 (1985).

[5] U. Tinivella, M. Peressi, and A. Baldereschi, J. Phys.: Condens. Matter **9**, 11 141 (1997).

[6] M. Exner, H. Donnerberg, C. R. A. Catlow, and O. F. Schirmer, Phys. Rev. B **52**, 3930 (1995); J. Phys.: Condens. Matter **6**, 3379 (1994).

[7] J. L. Martins and A. Zunger, Phys. Rev. B **30**, 6217 (1984).

[8] J. C. Woicik, K. E. Miyano, C. A. King, R. W. Johnson, J. G. Pellegrino, T. L. Lee, and Z. H. Lu, Phys. Rev. B **57**, 14 592 (1998).

[9] J. C. Mikkelson and J. B. Boyce, Phys. Rev. B **28**, 7130 (1993).

[10] G. M. Lamble, R. J. Reeder, and P. A. Northrup, J. Phys. IV **7**, 793 (1997); R. J. Reeder, G. M. Lamble, and P. A. Northrup, Am. Mineral. **84**, 1049 (1999). These studies reported conserved first-shell distances within uncertainty from single-shell fits, but marginally larger ones from multiple-shell fits involving multiple scattering.

[11] L. Cheng, N. C. Sturchio, J. C. Woicik, K. M. Kemner, P. F. Lyman, and M. J. Bedzyk, Surf. Sci. **415**, 976 (1998).

[12] L. Cheng, N. C. Sturchio, and M. J. Bedzyk, Phys. Rev. B **61**, 4877 (2000).

[13] L. Cheng, N. C. Sturchio, and M. J. Bedzyk (unpublished).

[14] For example, F. K. Hurd, M. Sachs, and W. D. Hershberger, Phys. Rev. **93**, 373 (1954); G. E. Barberis, G. B. Martins, and R. Calvo, Phys. Rev. **49**, 8583 (1994).

[15] G. Yang, J. K. Furdyna, and H. Luo, Phys. Rev. B **62**, 4226 (2000).

[16] W. Stumm, *Chemistry of the Solid-Water Interface* (Wiley, New York, 1992).

[17] M. J. Bedzyk and G. Materlik, Phys. Rev. B **32**, 6456 (1985).

[18] M. J. Bedzyk and G. Materlik, Surf. Sci. **152**, 10 (1985).

[19] H. Effenberger, K. Mereiter, and J. Zemann, Z. Kristallogr. **156**, 233 (1981).

[20] D. E. Sayers and B. A. Bunker, in *X-ray Absorption*, edited by D.

C. Konigberger and R. Prins (Wiley, New York, 1988); S. S. Hasnain, *X-ray Absorption Fine Structure* (Ellis Horwood, New York, 1991).

[21] C. Bouldin, L. Furenlid, and T. Elam, Physica B **208-209**, 190 (1995).

[22] S. I. Zabinsky, J. J. Rehr, A. Ankudinov, R. C. Albers, and M. J. Eller, Phys. Rev. B **52**, 2995 (1995).

[23] E. A. Stern, M. Newville, B. Ravel, Y. Yacoby, and D. Haskel, Physica B **208-209**, 117 (1995).

[24] The effects of multiple scattering in the $MnCO_3$ and the $CaCO_3:Mn^{2+}$ data were examined; inclusion of the most significant multiple scattering path in the models did not improve the fits or change their results.

[25] B. W. Batterman, Phys. Rev. Lett. **22**, 703 (1969); J. A. Golovchenko, B. W. Batterman, and W. L. Brown, Phys. Rev. B **10**, 4239 (1974).

[26] N. Hertel, G. Materlik, and J. Zegenhagen, Z. Phys. B: Condens. Matter **58**, 199 (1985).

[27] T. Gog, P. Schotters, J. Falta, G. Materlik, and M. Grodzicki, J. Phys.: Condens. Matter **7**, 6971 (1995).

[28] A. Kazimirov, L. Cao, G. Scherb, L. Cheng, M. J. Bedzyk, and J. Zegenhagen, Solid State Commun. **114**, 271 (2000).

[29] Y. Qian, N. C. Sturchio, R. P. Chiarello, P. F. Lyman, T. L. Lee, and M. J. Bedzyk, Science **265**, 1555 (1994).

[30] N. E. Pingitore, F. W. Lytle, B. M. Davies, M. P. Eastman, P. G. Eller, and E. M. Larson, Geochim. Cosmochim. Acta **56**, 1531 (1992).

[31] N. C. Sturchio, M. R. Antonio, L. Soderholm, S. R. Sutton, and J. C. Brannon, Science **281**, 971 (1998).

[32] A. Frenkel, E. A. Stern, A. Voronel, A. Qian, and M. Newville, Phys. Rev. Lett. **71**, 3485 (1993).

[33] V. Vikhnin, P. Voigt, and S. Kapphan, J. Phys.: Condens. Matter **7**, 7227 (1995).

[34] F. Despa, Phys. Status Solidi B **191**, 31 (1995).

[35] J. M. Zachara, C. E. Cowan, and C. T. Resch, Geochim. Cosmochim. Acta **55**, 1549 (1991).

[36] A. Pavese, M. Catti, S. C. Parker, and A. Wall, Phys. Chem. Miner. **23**, 89 (1996).

[37] D. K. Fisler, J. Gale, and R. T. Cygan, Am. Mineral. **85**, 217 (2000).